International Journal of Computational and Experimental Science and ENgineering (IJCESEN)

Vol. 11-No.3(2025)pp. 6973-6986
http://www.ijcesen.com

ISSN: 2149-9144

Research Article

Examining the Neutron and Gamma Attenuation Characteristics of Various Amorphous Structures with Bioactive Properties

Hasipcan AYDIN[1*], Gülfem SÜSOY DOĞAN[2], Hüseyin Ozan TEKİN[3,4], Duygu ŞEN BAYKAL[5], Yusuf Cenk İLTUŞ[6]

[1] Istanbul University, Institute of Graduate Studies in Sciences, Department of Physics, 34134, Istanbul, Türkiye
Corresponding Author Email: hasipcanaydin@gmail.com - **ORCID:** 0000-0002-4259-6944

[2] Istanbul University, Faculty of Science, Department of Physics, 34134, Istanbul, Türkiye
Email: susoy@istanbul.edu.tr - **ORCID:** 0000-0002-3760-1999

[3] Department of Medical Diagnostic Imaging, College of Health Sciences, University of Sharjah, 27272, Sharjah, U.A.E.
[4] Istinye University, Faculty of Engineering and Natural Sciences, Computer Engineering Department, 34396, Istanbul, Türkiye
Email: htekin@sharjah.ac.ae - **ORCID:** 0000-0002-0997-3488

[5] Istanbul Nisantasi University, Mechatronics Engineering, Faculty of Engineering and Architecture, 34398, Istanbul, Türkiye
Email: duygushenn@gmail.com - **ORCID:** 0000-0001-9833-9392

[6] Istanbul University, Institute of Graduate Studies in Sciences, Department of Physics, 34134, Istanbul, Türkiye
Email: yusufcenkiltus@gmail.com - **ORCID:** 0000-0002-3749-8047

Article Info:

DOI: 10.22399/ijcesen.2176
Received : 10 July 2025
Accepted : 15 September 2025

Keywords

Radiation Protection;
Gamma-ray;
Neutron;
Bioactive Amorphous Glass;
PHITS code.

Abstract:

Bioactive glasses are silicates that have phosphorus, calcium, and sodium in them. These glasses were created to help or carry out essential functions in the living tissues of the human body. The exceptional mechanical and physical properties of bioactive glasses make them suitable for radiation protection. Despite the costs and risks, lead (Pb) and traditional concrete are still the most effective radiation protection materials. Bioactive glass materials are considered to be effective due to their non-toxicity, economic feasibility and practicality. This study presents the neutron and gamma shielding properties of thirteen bioactive amorphous glass samples that are divided into three groups. The mass attenuation coefficient, represented by (μ_m), for the selected bioactive glasses was calculated using the Phy-X/PSD program in the photon energy range of 0.02 to 15 MeV. The μ_m was also used to evaluate other important metrics for the selected bioactive glasses, including the half and tenth value layer (HVL and TVL), mean free path (MFP), effective atomic number (Z_{eff}), and effective electron number (N_{eff}). The transition factors (TFs) of bioactive amorphous materials, whose radiation shielding parameters were calculated theoretically, were simulated at three energies by PHITS (Particle and Heavy Ion Transport Code System). In particular, the FPG6 exhibits a discernible decrease in TF values among the CaF-doped samples, demonstrating their improved radiation-shielding capability, with a MAC value of 0.01961 cm²/g. When compared to other bioactive glasses, it is clear that FPG6 sample has the lowest HVL, TVL, and MFP values. For instance, for an energy value of 15 MeV, the HVL value of FPG6 is 12.02966 cm. To evaluate the neutron protection properties of the bioactive glasses under study, effective removal cross-section values (ΣR) have been developed. The results show that BG4B has exceptional neutron attenuation capabilities, with a value of 0.11 cm^{-1}.

1. Introduction

Since the discovery of the first bioactive glass-ceramic 45S5 Bioglass by Hench et al. (1971) [1] near the end of the 1960s, many different types of

chemicals have been documented [2], [3], [4]. Medical implants, dental care, and scaffolds for tissue engineering are just a few of the many applications for these bioactive glasses [5], [6]. The oxide metals silicon dioxide (SiO_2), sodium oxide (Na_2O), calcium oxide (CaO) and phosphorous oxide (P_2O_5) are frequently utilised in the manufacture of bioactive glasses. In regeneration applications, it has been observed that replacing SiO_2 with B_2O_3, Na_2O with K_2O, or CaO with CaF_2/MgO increases the bioactivity of these glasses. [7], [8]. Glass-ceramic and biomaterial-based surface-reactive materials can be categorized as bioactive glass [9]. Several testing techniques have shown in recent decades that bioactive glasses are extremely biocompatible. As a result of their novel material qualities and biocompatibility in living biological systems, they are now being considered as potential implant materials for surgical restoration or replacement procedures [10]. Bioactivity is the capacity of a material to specifically attach to bone and strengthen bone structure. The degree of bioactivity of a substance is determined by its ability to provide a steady and regulated flow of chemical stimuli to promote tissue growth and cell function. The crystalline structure, chemical composition, and processing characteristics of bioactive substances regulate the rate at which new tissues develop and graft material resorbs [11]. A bioactive glass often has a structure based on calcium or silica [12]. Effective usage of bioactive glasses requires that they have mechanical qualities suitable for the environment in which they are used, be free of toxicity or cancer, not react (bioavailability), and not corrode in human fluids [13]. Because the crystalline ceramics and compositions in the Na_2O, CaO-P_2O_5-SiO_2 system, which are the basic building blocks of bioactive glasses, generate robust interactions with living tissues [1]. Tissues and implants interact chemically as a result of calcium and phosphorus replacing some silica groups in the bioactive glass structure [14]. Phosphate (P_2O_5) is included in the formulation of the bioactive glass to ensure its bioactivity. Because it has the ability to improve a certain biological reaction, characteristic, or function in the glass host. Because silicate has a high melting point, the glass composition melts completely, improving the manufactured glasses' uniformity [15]. Calcium phosphate-based bioactive glasses typically have a high mechanical strength. A battery of mechanical tests is performed on bioactive glasses. Glass's mechanical strength increases as its crystallization increases, or moves away from its amorphous structure, but its biodegradable quality vanishes [16]. The mechanical characteristics of the bioactive glasses should be as close as possible to those of the tissue of interest, so as to avoid any interference with the patient's regular everyday activities. Radiation is currently the greatest threat to both humans and the environment. The development of suitable substitute shielding materials is required due to the increasing use of radiation in numerous fields. Despite being ineffective, expensive, and dangerous for neutron shielding, lead (Pb) and conventional concrete are currently believed to be the best shielding materials. Much work has been done thus far to create radiation shielding materials that are economical, non-toxic, useful, and effective. The following materials have been offered as competing radiation shielding materials: commercial glasses, HMO glasses, alloys, concretes, and rocks [17], [18], [19], [20], [21]. There have been numerous proposals recently for the use of additive-doped bioactive glasses in radiation protection applications [22], [23], [24], [25]. The application of bioactive glasses for radiation protection is highly appealing due to its mechanical qualities, amorphous shapes, and light weight. Additionally, the outcomes of the radiation attenuation characteristics for the glasses might help in selecting the right bioactive glass for the human body [26], [27]. Bioactive glasses need further study and development to reach their full potential, notwithstanding their benefits in radiation shielding applications. The manufacture, bioactivity, and biodegradability of bioactive glasses have all been the subject of several studies [28], [29] but there are currently few investigations [30], [31], [32] on their capacity to shield against radiation, necessitating further thorough research. To this end, thirteen bioactive glass samples were analysed as three distinct mixes. There were three groups of bioactive glass samples that were analysed: the BGXB group, the SRY group, and the FPGZ group. SiO_2-Na_2O-CaO-P_2O_5-B_2O_3 was chosen as the basis glass for the first composition. Five different B_2O_3 modified glass compositions, known as BG0B, BG1B, BG2B, BG3B, and BG4B were produced by replacing SiO_2 with B_2O_3 in the basic glass composition [33]. It has been shown that borate-based glasses, as well as silicate-based bioactive glasses, have faster rates of dissolution and surface apatite production [34]. Another advantage of these glasses is that they can be used to modify the pace of apatite formation in accordance with the host bone-tissue metabolism. This allows for controlled breakdown of the glasses, which leads to a progressive replacement of bone [35]. It should be noted that boron is crucial for bone health and that numerous research teams have already documented trace levels of this element in healthy human bones [36], [37], [38], [39], [40]. For the second mixture, the base glass was selected as (P_2O_5-CaO-Na_2O-K_2O-SrO) with varying percentages [41] named as SR5 - SR10 - SR15. Glass ceramics and glasses

made of calcium phosphate have attracted interest for medical applications due to their unique properties. By integrating with bone and generating a physiologically active hydroxyapatite layer at the implant/bone contact, a bioactive calcium phosphate-based implant in particular facilitates bonding with soft tissues and bone [27], [46]. In aquatic conditions, glasses become extremely reactive due to the creation of non-bridging oxygens (NBOs) and network disorders caused by the addition of cations or network modifiers such as Ca, Na or K. Applications involving bone augmentation and repair now significantly benefit from this high responsiveness. Numerous interesting investigations have been conducted on glass ceramics and bioactive glasses that become even more bioactive with the addition of SrO [47], [48], [49]. Lastly, phosphate-based glasses with varying fluoride contents were employed, (P_2O_5-CaO-Na_2O-CaF_2) with varying percentages [50] named as FPG0 - FPG1 - FPG2 - FPG3 - FPG6. When it comes to encouraging bone production in the human body, fluoride is usually the most promising ingredient in physiological solutions. This mixture focuses on the effects of CaF_2 as a nucleating agent in the P_2O_5-CaO-Na_2O glass system [51]. We looked into these glasses for radiation shielding applications because such qualities are desirable and intriguing while creating new shielding materials. The PHITS (Particle and Heavy Ion Transport Code System) code is used in this work to examine the ionizing gamma and neutron shielding properties of three sets of bioactive glasses with varying compositions of B_2O_3, SrO, and CaF_2. The density and composition of the glasses under examination are compiled in Table 1. Certain parameters can be used to determine the radiation shielding properties in the wide energy range of 0.02-15 MeV, including the transmission factors (TFs), effective atomic number (Z_{eff}), effective electron number (N_{eff}), half and tenth value layer (HVL and TVL), mean free path (MFP), and mass attenuation coefficient (MAC, μ_m) [19]. The (μ_m) values for the selected bioactive glasses were calculated in the photon energy range of 0.02 to 15 MeV using the Phy-X/PSD [52]. The transition factors (TFs) of bioactive amorphous materials, whose radiation shielding parameters were calculated theoretically, were simulated at three energies by PHITS code [53], [54]. Figure 1 shows the PHITS configuration for TF computations in three dimensions. Furthermore, effective removal cross-sections values (ΣR) [19] have been established in order to assess the neutron protection ability of the bioactive glasses under investigation. The removal cross-section (ΣR) of the glasses was estimated. The current glasses' characteristics were found to be within the same range as those of materials utilized for shielding against neutrons and gamma rays. Additionally, the bioactive glasses' neutron shielding properties were evaluated.

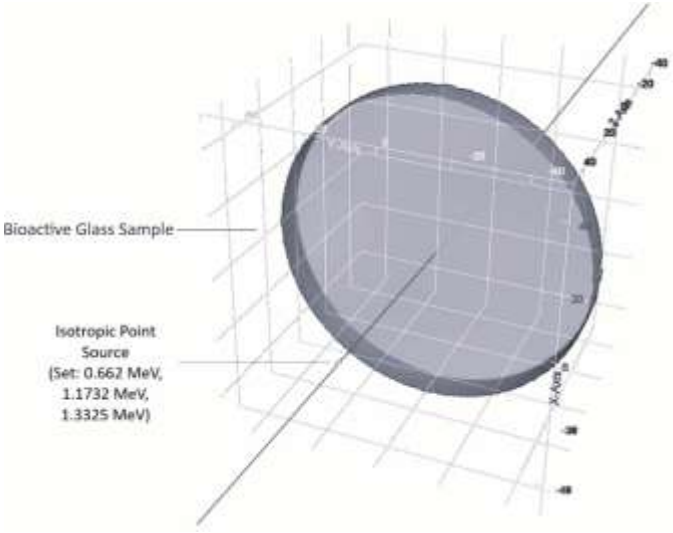

Figure 1. *A total-3D view of designed simulation geometry by using PHITS code for photon transmission factor (TF) studies*

2. Material and Methods

The physical characteristics of the shielding materials must be established before radiation protection applications can be implemented. The following equation 1 expresses the Beer-Lambert law, which is employed in the attenuation of γ-ray radiation [21]:

$$I(x) = I_0 e^{-\mu x} \qquad (1)$$

The chance of attenuation is proportional to the matter's linear attenuation coefficient (μ), thickness (x), and density (ρ). The density dependency of the linear attenuation coefficient (μ) has been removed by introducing a second parameter known as the mass attenuation coefficient (μ_m), which is computed by dividing μ by the density of matter (ρ). Typically, cm^2/g is used to express it. Based on the mixture rule [52], Phy-X/PSD software [53], [54], [55], and [56] can produce data to compute the (μ_m) values for the specified glass samples in the continuous energy region (1 keV-15 MeV) [51]. The program gives cross sections and total and partial attenuation coefficients for a number of interaction processes, such as Compton scattering, Rayleigh scattering, photoelectric absorption, pair production in nuclear and electric fields, and more, for about 100 elements. Equation (2) provides the mass attenuation coefficient (μ_m) formula [21], [22].

$$\mu_m = \frac{\mu}{\rho} \qquad (2)$$

Table 1. *Chemical properties and densities of the All-Group Bioactive Amorphous Glass Samples*

Sample ID	P_2O_5	Na_2O	CaO	SiO_2	B_2O_3	K_2O	SrO	CaF_2	Density (g/cm^3)
BG0B	1.72	22.70	21.77	53.85	0	0	0	0	2.660
BG1B	1.72	22.70	21.77	40.39	13.46	0	0	0	2.640
BG2B	1.72	22.70	21.77	26.925	26.925	0	0	0	2.630
BG3B	1.72	22.70	21.77	13.46	40.39	0	0	0	2.590
BG4B	1.72	22.70	21.77	0	53.85	0	0	0	2.540
SR5	59.50	20.00	17.00	0	0	3.00	0.50	0	2.654
SR10	59.00	20.00	17.00	0	0	3.00	1.00	0	2.604
SR15	58.50	20.00	17.00	0	0	3.00	1.50	0	2.596
FPG0	48.00	32.0	20.00	0	0	0	0	0	2.718
FPG1	48.00	31.0	20.00	0	0	0	0	1.00	2.662
FPG2	48.00	30.0	20.00	0	0	0	0	2.00	2.690
FPG3	48.00	29.0	20.00	0	0	0	0	3.00	2.701
FPG6	48.00	28.0	20.00	0	0	0	0	4.00	2.708

The linear attenuation coefficient is denoted by μ, while the shielding material's density is represented by ρ. It is the essential instrument for determining a wide range of other parameters, including the electron density, effective atomic number, electronic cross-section, molecular cross-section and atomic cross-section. A photon's mean free path, or MFP, is the average distance it can travel through a substance before coming into contact with an event. Using the relation below, the mean free path has been determined using the linear attenuation coefficient [21];

$$MFP = \frac{1}{\mu} \qquad (3)$$

The TVL and HVL of a given material are the thicknesses at which 10% and 50% of the primary energy is attenuated, respectively. The most widely used raw parameter for characterizing a glass system's radiation shielding effectiveness is the HVL. Equations 4 and 5 are used to determine the HVL and TVL using the linear attenuation coefficient (μ) [21], [22].

$$HVL = \frac{In2}{\mu} \qquad (4)$$

$$TVL = \frac{In10}{\mu} \qquad (5)$$

The shielding capabilities of the glass samples are improved when gamma photon interactions with it is more effective, as indicated by a low MFP, HVL or TVL value.

One important factor in the radiation absorption of compounds, mixes, and alloys is the effective atomic number (Z_{eff}). Clearly, not all energies exhibit the typical energy of the atomic number of elements. This is due to the change in photon interaction in the composite material's cross section. For composite materials, the phrase "atomic number" has been used, and it is said that this value varies with energy. The effective atomic number [57] is theoretically determined by dividing the total $\sigma_{t,a}$ (atomic cross-section) by the $\sigma_{t,el}$ (total electronic cross-section) derived in Equation 6 [63].

$$Z_{eff} = \frac{\sigma_{t,a}}{\sigma_{t,el}} \qquad (6)$$

Based on the atomic number (Zi), atomic weight (Ai), and mole fraction (fi) values of the constituent elements, the effective atomic number (Zeff) has been calculated using the following formula [57].

$$Z_{eff} = \frac{\sum_i f_i A_i (\mu/\rho)_i}{\sum_i f_i \left(\frac{A_i}{Z_i}\right)\left(\frac{\mu}{\rho}\right)_i} \qquad (7)$$

The Z_{eff} is a frequently used parameter for radiation protection, dosage estimations, and diagnosis and treatment, particularly in nuclear medicine. The electron density and the effective electron number have comparable applications [63]. Effective electron number indicates the number of electrons interacting with the substance per unit mass [57], [58].

$$N_e = \frac{N_A Z_{eff}}{\langle A \rangle} \qquad (8)$$

The average atomic weight ⟨A⟩, or average atomic mass, can be expressed as Equation 9 [59], [60].

$$\langle A \rangle = \frac{M}{\sum_i n_i} \qquad (9)$$

When an elemental material has several structures, the electron density is represented by N_{eff} using the following formula [21].

$$N_{eff} = N_A \frac{Z_{eff}}{<A>} \qquad (10)$$

Measures such as electron density (N_{eff}) and effective atomic number (Zeff) are used to characterize the response of multi-elemental systems to ionizing radiation. Numerous technical and

industrial applications, such as radiation shielding, absorption dose calculations, and photon multiplication factor calculations, frequently make use of these properties. These are the parameters calculated to show the importance of the gamma and X-ray absorption rates of the materials used. The Zeff and N_{eff} values have a linear connection and change according to the source photon's energy. [62]. In addition to calculating the mass attenuation coefficients, the transmittance factors (TFs) depending on the photon energy for each glass sample were also investigated. Using PHITS simulations, gamma-ray transmission through the composite materials was modelled [53]. PHITS uses Monte Carlo techniques to model the passage of gamma radiation through materials and perform TF calculations at three different energies (0.662 MeV, 1.1732 MeV, and 1.3325 MeV) for various material thicknesses. The simulations, which were conducted by creating an isotropic point source and tracking photon interactions across the simulated samples, produced radiation attenuation characteristics at different energy levels. The TF values of samples T(E,d) in a specific gamma (E) energy are given by Equation 11 [58].

$$T(E,x) = \frac{F(E,x)}{F(E,0)} \qquad (11)$$

One of the key numbers for estimating neutron shielding is the fast neutron effective removal cross section (ΣR). The ΣR values for fast neutrons for the studied materials were calculated using the following formulas [58].

$$\Sigma_{R/\rho} = \sum_i w_i (\Sigma_{R/\rho})_i \quad (12)$$

$$\Sigma_R = \sum_i \rho_i (\Sigma_{R/\rho})_i \qquad (13)$$

where w_i shows the weight fraction of the i component and ρ_i is the density of the sample.

3. Results and Discussions

Materials' composition and structural qualities have a big impact on how well they absorb radiation. The ability of a material to attenuate radiation can be impacted by compositional changes, such as the insertion of dopants or adjustments to elemental ratios, which alter the atomic arrangement and bonding inside the material. The radiation-attenuating properties of three sets of bioactive glass samples with different B_2O_3, SrO, and CaF_2 doping concentrations are investigated in this work.

3.1. Mass attenuation coefficients (MAC) of the bioactive glasses under examination

High-density materials are thought to be better for shielding against gamma rays since they have a higher atomic number. In addition to the chemical component of glasses, the MAC is mostly linked to photon energy, which explains this. The characteristics of changes in MAC values for photon energy are comparable. As per the Beer-Lambert rule, the MAC values for every glass sample exhibit greater magnitude at low photon energies (≤0.1 MeV) and then decline exponentially with increasing photon energy. The photon is attenuated throughout the energy zone by three distinct mechanisms. In the low energy range of 10–100 keV, the photoelectric process is crucial. The cross-section of the photoelectric effect is strongly influenced by the atomic number of an element (Z^{4-5}) and the gamma ray energy ($E^{-3.5}$). This process is followed by Compton scattering, which is significant in the mid-energy region between 0.1 and 10 MeV. The Compton scattering process's cross-section gradually drops as gamma-ray energy increases and is least reliant on atomic number. For all elements, this mechanism is hence predominant at intermediate photon energy. Finally, pair production is the predominant activity in the high energy region over 10 MeV energy. The atomic number Z^2 and photon energy log(E) have a linear relationship with the cross-section for pair production. These energy ranges vary slightly depending on the type of material.

Phy-X/PSD software was used to calculate the MAC values for the selected bioactive glass samples. The MAC values, (cm^2/g) of three sets of bioactive glass samples are shown graphically in Figure 2, Figure 3 and Figure 4 for a range of photon energy (from 0.015 MeV to 15 MeV). According to figures, it can be clearly seen that the MAC values for each bioactive glass sample decrease rapidly as the energy of gamma rays increases between 0.02 and 0.6 MeV. This sharp decline is caused by the photoelectric effect, which predominates in low energy region. The BG0B material has the highest MAC value among the BGXB group materials, especially in the low energy zone, while the BG4B material has the lowest, as the graph makes evident. This is because the molar contribution of SiO_2 is dominant in the BG0B material and the material density is high. In the SRY group material example, the SR15 material has the highest MAC value due to the dominant molar contribution of SrO. Despite having a low density, the SR15 material's greater MAC value in this energy range can be explained by the photoelectric cross section being proportional to Z^5. On the other hand, in the FPGZ group material example, the FPG6 material has the highest MAC value due to the dominant CaF_2 contribution and the material density is high. Because of the considerable

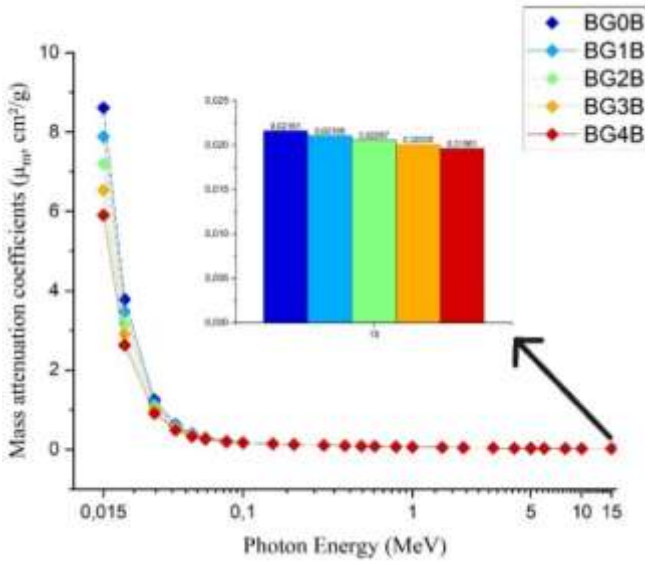

Figure 2. *Mass attenuation coefficients (μ_m, cm^2/g) of BGXB group bioactive amorphous glass samples with photon energy from 0.02 to 15 MeV.*

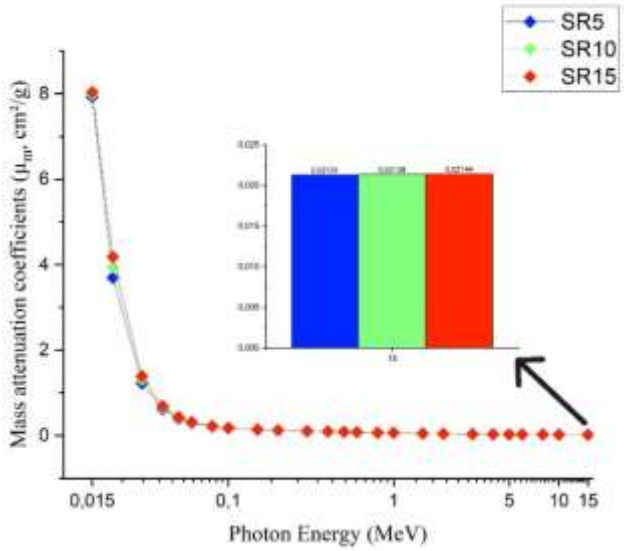

Figure 3. *Mass attenuation coefficients (μ_m, cm^2/g) of SRY group bioactive amorphous glass samples with photon energy from 0.02 to 15 MeV.*

influence of the Compton interaction, the MAC values rapidly decrease in the intermediate energies of 0.1-1 MeV. Furthermore, the atomic number, Z, of the interacting atom determines the Compton scattering cross section. MAC values stay the same up to roughly 5 MeV. Nevertheless, the pair production procedure influences the MAC values, which are almost constant for all glass samples over 1 MeV. The Z atomic number squared has a relationship with the pair formation coefficient. It was found that the MAC values in the pair formation zone were very close to each other for all the materials examined. It was evident how the material density and the MAC values of the materials under investigation related to one another.

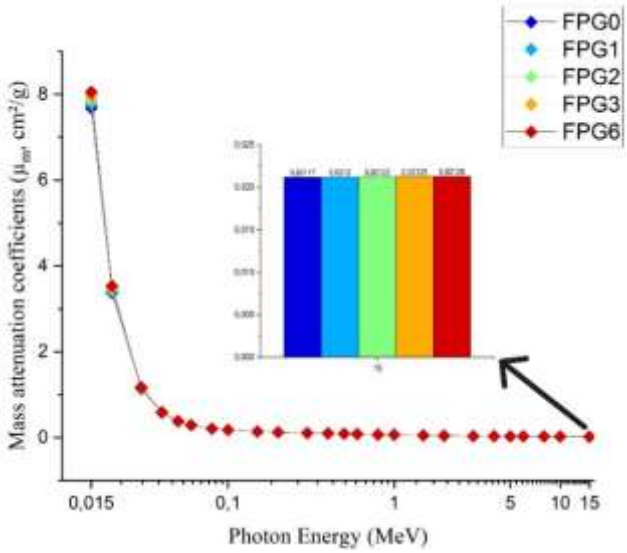

Figure 4. *Mass attenuation coefficients (μ_m, cm^2/g) of FPGZ group bioactive amorphous glass samples with photon energy from 0.02 to 15 MeV.*

A comparison of all the samples examined is shown in Figure 5. In the low energy range, the SR15 sample has the greatest MAC value, as seen in Figure 5. At high and medium energies, the FPG6 sample with the highest density shows the dominant feature in terms of MAC value.

As we get closer to the high-energy zone, the attenuation coefficients smooth out and then gradually drop, suggesting that Compton scattering is the main interaction mechanism (beyond 0.6 MeV). As energy increases, the differences in attenuation capacities between the various compositions diminish, highlighting the necessity of selecting appropriate glass materials for shielding based on the desired energy range. All samples' MAC values continue to decline in the high-energy zone, and attenuation from pair creation begins to show up, however considerably less prominently for the specified glass samples in these energy ranges. The relevant measurements were carried out at values corresponding to the MAC experiment. A quantitative metric called the MFP is used to calculate the average distance a photon travels through a substance in the absence of interactions. [57]. The mean free path values for all materials are found to be almost the same in the low energy region, where the photoelectric effect's cross section is high. On the other hand, FPG6 is the glass material with the lowest MFP value when the energy level rises, that is, in the energy range where the Compton scattering and pair creation rate are large. The thicknesses at which the radiation intensity decreases by 50% and 10% respectively, are the HVL and TVL. These are important factors to consider when assessing a material's radiation shielding capabilities. In samples containing

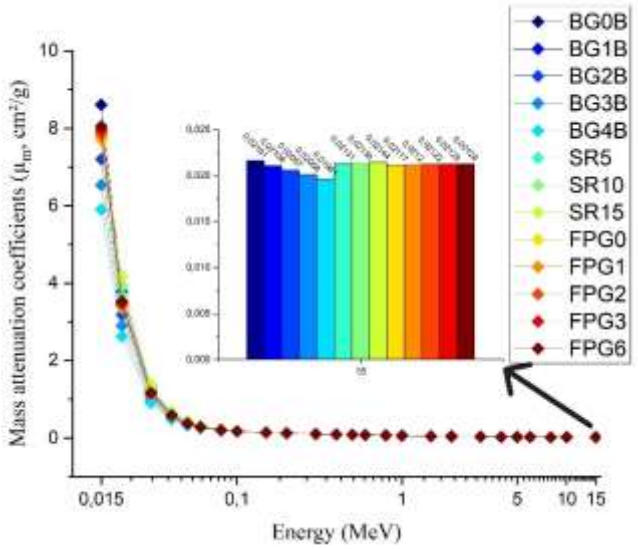

Figure 5. *The relationship between photon energy (MeV) and Mass attenuation coefficients (μ_m, cm^2/g) of all investigated glasses*

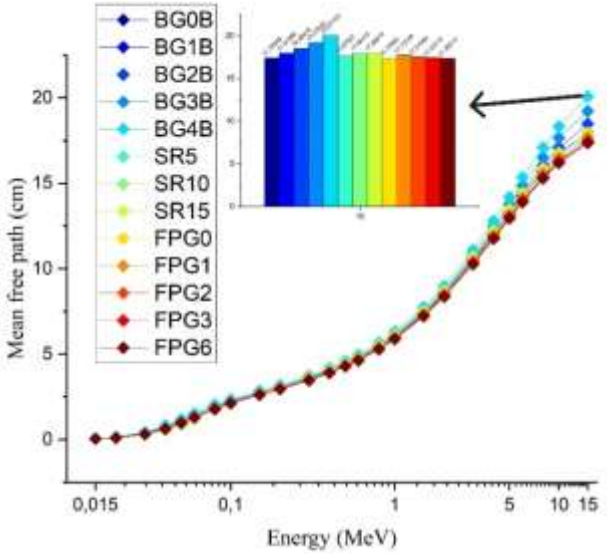

Figure 6. *The relationship between photon energy (MeV) and mean free path (cm) for all investigated glasses*

predominantly phosphorus, sodium and calcium, a relatively similar HVL and TVL was observed across the range of low-energy values [57]. This finding suggests that the attenuation characteristics within this specific group are consistent, indicating a uniform response in this particular composition.

HVL and TVL values, however, rapidly rise with increasing energy level, particularly in the low energy region where the photoelectric effect predominates. This implies that to attain the same degree of radiation attenuation, the glass samples need a thicker coating. The HVL and TVL values for all samples start to converge as the energy level rises, which may be seen as a reflection of Compton scattering and the photoelectric effect's declining impacts. For all glass samples, the HVL and TVL values stabilize at higher energies, specifically over 10 MeV. This finding suggests that pair creation emerges as a key interaction mechanism at these energies. The lowest HVL and TVL values for each group of glasses (BGXB, SRY and FPGZ) in the low and high energy ranges were obtained for the BG0B, SR5 and FPG6 bioactive glass samples, respectively, indicating better shielding efficiency. Furthermore, the B-doped glass material with low electron density demonstrated that thicker glass armouring is required at the same energy level. It can be inferred that the attainment of a comparable degree of radiation attenuation in these glasses necessitates the implementation of a more substantial layer, potentially attributable to the diminished presence of elements with lower atomic numbers within these samples in contradistinction to the Si-doped series.

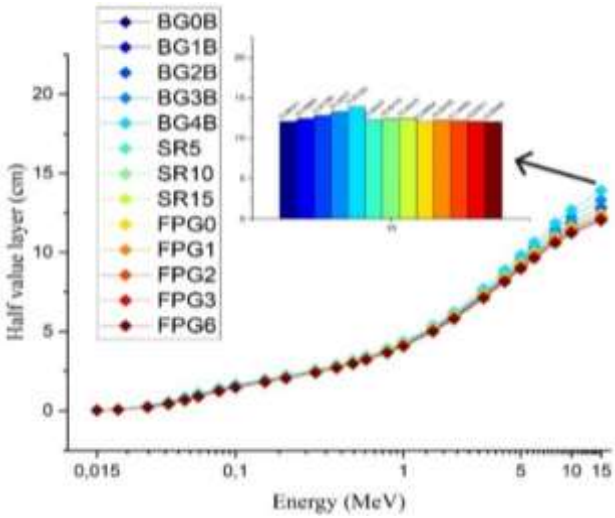

Figure 7.a) *The relationship between photon energy (MeV) and half value layer (cm) for all investigated glasses*

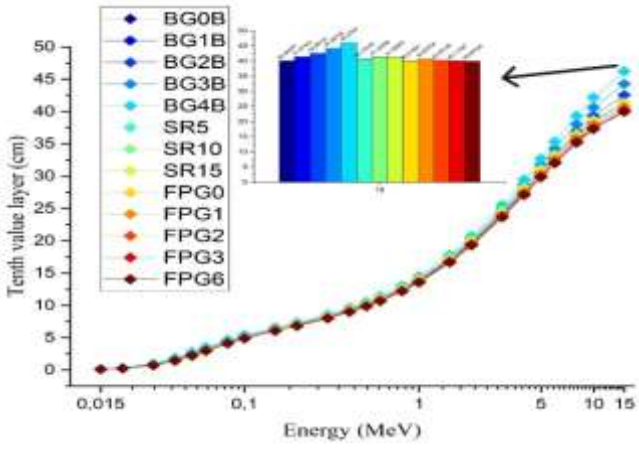

Figure 7.b) *The relationship between photon energy (MeV) and Tenth value layer (cm) for all investigated glasses*

3.3. Effective atomic (Z_{eff}) and effective electron (N_{eff}) numbers of the bioactive glasses under examination

Figures 8 and 9 display the changes in the (Z_{eff}) and (N_{eff}) values of the bioactive glass samples with energy. Higher Z_{eff} values indicate improved attenuation capabilities, making Z_{eff} a crucial parameter in assessing the photoelectric effect [57]. As shown in Figure 8, bioactive glasses with Sr content have higher Z_{eff} values at lower energies due to the dominant molar contribution. This finding indicates enhanced photoelectric absorption. It has been demonstrated that the effect weakens with rising energy, as the dominance of Compton scattering increases. As demonstrated in Figure 9, a notable disparity emerges in the N_{eff}, a critical factor for the comprehension and prediction of the Compton scattering phenomenon, when analysing different types of bioactive glass. As can be clearly seen from the figure, the N_{eff} values of BGXB series glass samples doped with elements with high atomic numbers are higher in the low energy region. More photon-electron interactions are made possible by the higher electron density, which is the cause of this phenomena. For every sample that is analysed, the N_{eff} values typically drop as the energy levels increase. This decrease suggests that Compton scattering is less likely to occur at higher photon energy. According to the results of both figures, adding heavy components significantly improves the glass's ability to interact with lower-energy radiation. This is evidenced by an increase in photoelectric absorption, as indicated by a higher Z_{eff}.

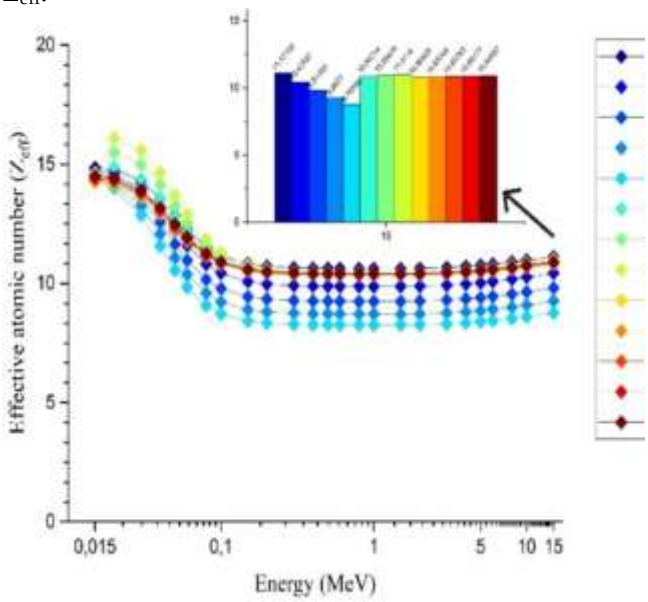

Figure 8. *The relationship between photon energy (MeV) and effective atomic number (Z_{eff}) for all investigated glasses*

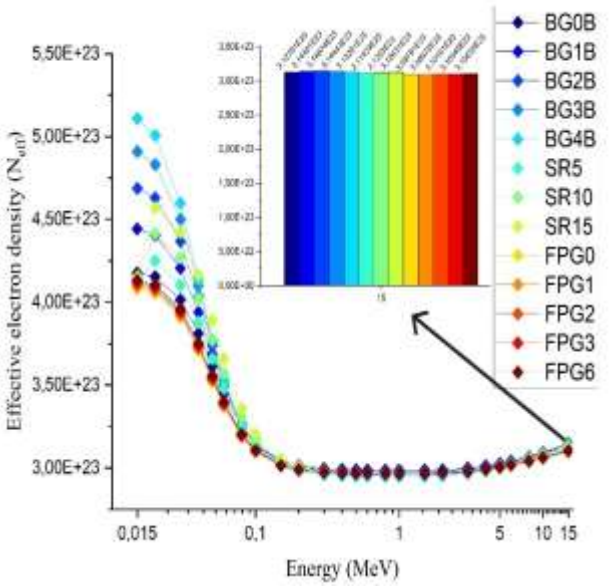

Figure 9. *The relationship between photon energy (MeV) and effective electron density (N_{eff}) for all investigated glasses.*

It has been shown that the elemental compositions of the various bioactive glass samples are directly correlated with the differences in N_{eff} and Z_{eff}.

Rising values of Z_{eff} and N_{eff} are directly correlated with increasing SrO content. In contrast, neither Z_{eff} nor N_{eff} are significantly increased when lighter calcium fluoride (CaF_2) is substituted. This is consistent with what would be predicted given the lower atomic numbers of fluorine (Z=9) and calcium (Z=20).

The bioactive glass samples' ability to attenuate gamma radiation was next assessed using the TF. We evaluated the bioactive glass samples' energy-dependent shielding behaviour by combining a wide variety of gamma-ray energies. This method allows for a detailed understanding of how different densities and compositions influence the material's ability to attenuate gamma rays with varying energy levels. Each bioactive glass sample's elemental mass fractions and densities were used to define its substance (see Table 1.).

Values for the Transmission Factor (TF) were computed for sample thicknesses between 0.5 and 3.0 cm. Six Figures show (from figure 10.a to figure 10.c) the variation in density values for the various sample mixtures. As the graph shows, the TF values for each energy level tended to decrease as the material thickness grew. This effect happens naturally and may be anticipated for almost any kind of material because the thickness of the material increases the number of photons absorbed. However, it was also discovered that the materials' TF factor values increased as the energy level increased. This indicates that as radioisotope energy increased, so did the gamma ray's penetrating capabilities and the intensity of secondary gamma-rays.

The opposite would also lead to a lower TF value if there were fewer secondary gamma rays, as shown in Equation 11. One possible explanation for this could be that fewer gamma rays can penetrate thick materials than thin ones. At all energy levels, the TFs typically exhibit a step drop for each of the three radioisotope energies as sample thickness increases. This behaviour demonstrates the bioactive glasses' efficient attenuation capabilities.

As sample thickness increased, all samples' TF values decreased, regardless of energy level. Higher photon energies, like 1.3325 MeV, are expected to have higher TF values than lower energies, like 0.662 MeV, since high-energy photons can penetrate more easily. This discrepancy becomes particularly noticeable at 3.0 cm, the maximum thickness, especially for the TF values that change with material thickness.

The total TF values indicate reduced attenuation efficacy at higher energies, slightly exceeding those at 0.662 MeV for the same thickness. The CaF-doped samples, especially the FPG6, show a very noticeable drop in TFs, which is indicative of their enhanced radiation shielding capacity. The graph's greater gradient for the FPG6 sample suggests that it has a noteworthy ability to absorb low-energy photons. All specimens exhibit the decreasing trend in the TFs with increasing thickness as the energy rises to 1.1732 MeV and 1.3325 MeV, albeit with less steepness than at lower energies.

This result implies that the CaF-doped glasses' relative attenuation capacity shows a minor decline at higher photon energy, even if they still function effectively. However, the FPG6 sample continues to show a lower TF than its rivals, which further supports its efficacy over a wider range of energies.

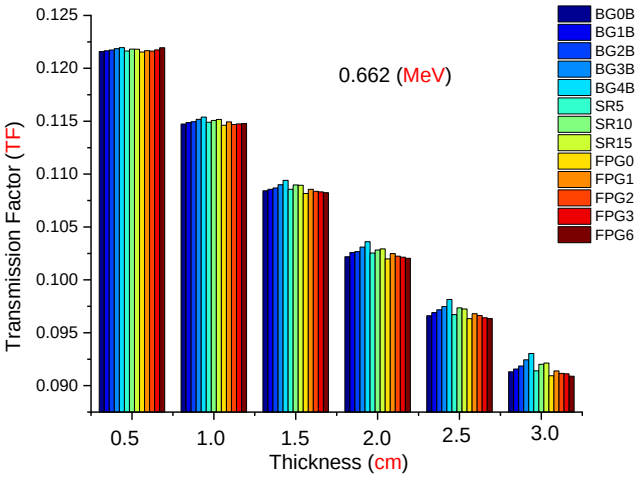

Figure 10.a. *Transmission factors (TF) for all glasses examined as a function of 0.662 MeV radioisotope energy for different sample thicknesses*

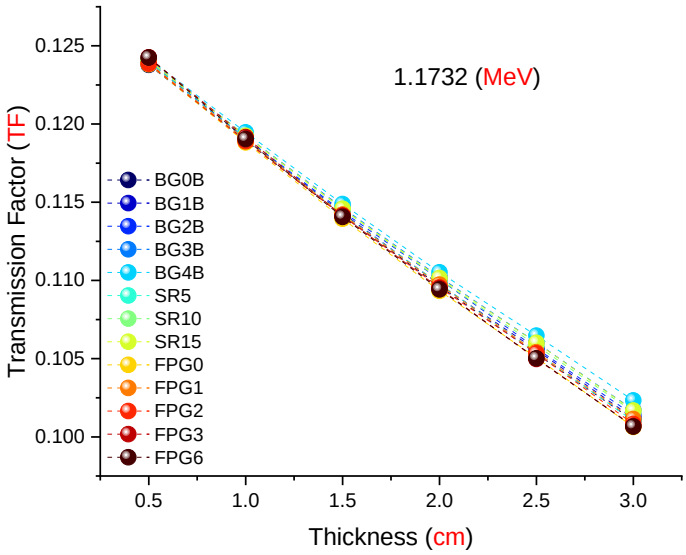

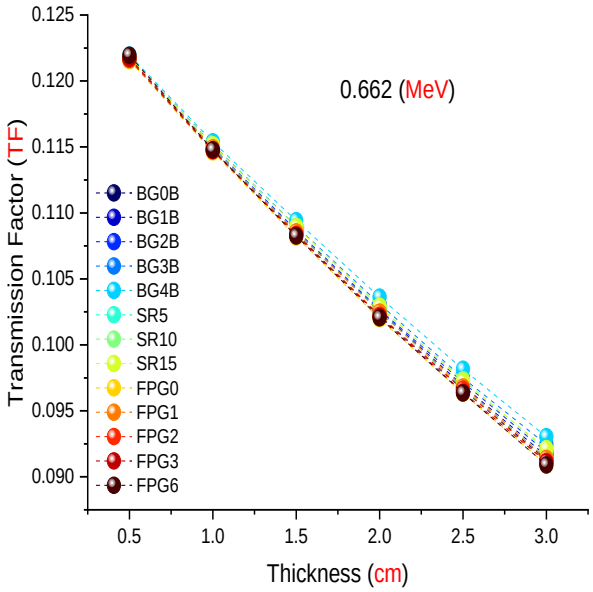

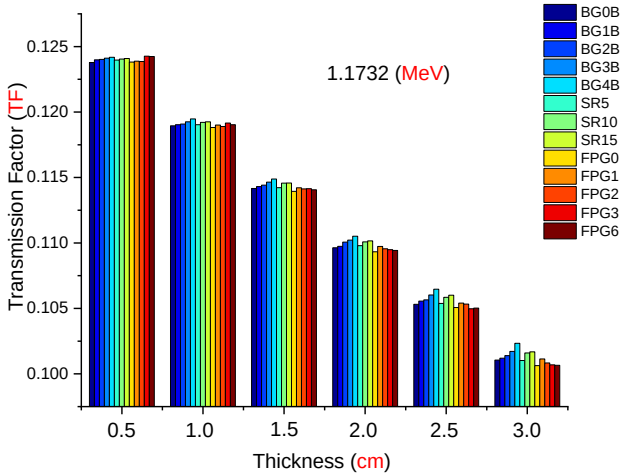

Figure 10.b. *Transmission factors (TF) for all glasses examined as a function of 1.1732 MeV radioisotope energy for different sample thicknesses*

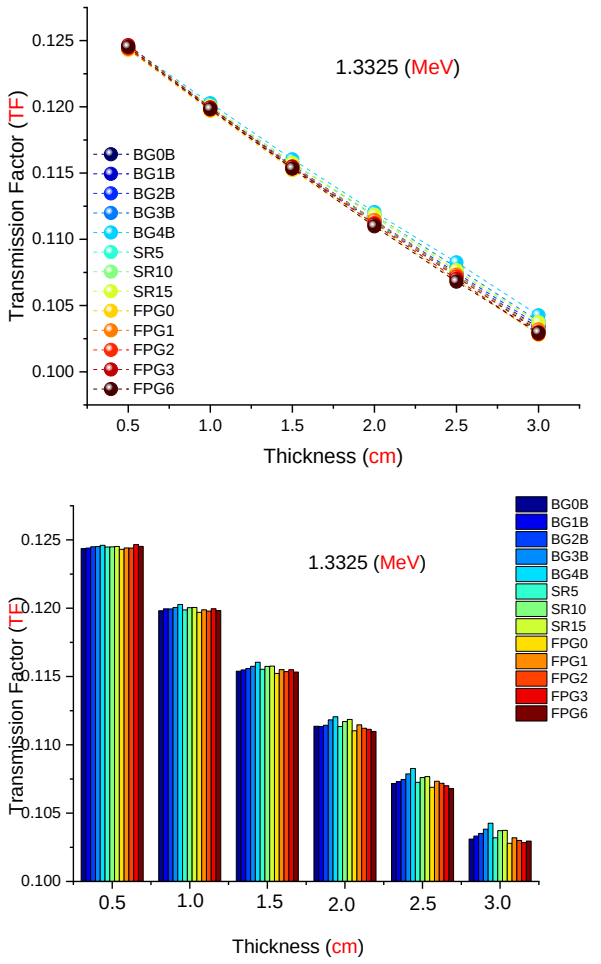

Figure 10.c. *Transmission factors (TF) for all glasses examined as a function of 1.3325 MeV radioisotope energy for different sample thicknesses*

3.5. Fast neutron removal cross sections (Σ_R) for values for the bioactive glasses under examination

Figure 11 displays the partial density values, basic components, and effective removal cross-section (ΣR) results for each bioactive glass. The increase in Σ_R indicates that the glass samples having higher B content are more effective at removing fast neutrons. As a result, adding B to the glass samples under study significantly improves their capacity to attenuate neutrons. By using the knowledge of (Σ_R/ρ), Σ_R can be analysed. Rapid neutron protection relies heavily on density, as seen in Figure 11, and BG4B is shown to have the highest value among the samples. The high Σ_R values observed in the BGXB group glass samples indicate that boron increases the neutron interaction due to its high neutron absorption cross section.

4. Conclusions

In this paper, the interaction parameters of three groups of bioactive glass samples, totalling thirteen, with photons and neutrons are examined. As mentioned before, the Phy-X/PSD software package

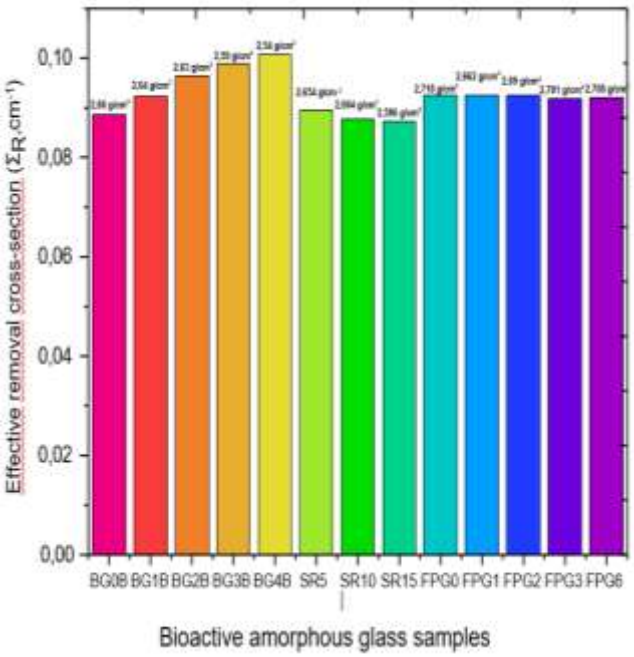

Figure 11. *Effective removal cross-section values of the bioactive amorphous glass samples with density*

was used to determine the MAC values. Based on the MAC data, the MFP, HVL, TVL, Z_{eff} and N_{eff} were calculated. Additionally, using the PHITS simulation, transition factors were computed at three energy values. The main results are listed below in accordance with the study's findings.

- A correlation between glass's chemical structure and its capacity to reduce ionizing radiation has been established by the current study. The investigation of the impact of the relevant components on physical characteristics including density, molecular weight, and effective atomic number provides proof of this.
- When compared to other glasses, the FPG6 glass has the lowest MFP, HVL and TVL values. The HVL value of FPG6 is 12.02966 cm for an energy value of 15 MeV.
- It is known that the density of the material affects the characteristics that characterize photon interaction.
- It has been discovered that Ca-doped glasses have greater effective atomic numbers and electron densities, which suggests better attenuation properties at higher photon energy.
- Additionally, the SR5 sample exhibited the lowest Z_{eff} values at low energy levels among the glass samples examined in three groups. However, in the low energy zone, the SR15 sample showed the greatest Z_{eff}

value. In other energy ranges (medium and high) the FPG6 sample has high Z_{eff} values.

- In the low energy range, BG4B glass sample exhibited highest N_{eff} values. Nevertheless, these values converged for all bioactive glass groups as the energy level rose.
- The enhanced radiation-shielding performance of the CaF-doped samples, particularly the FPG6, as investigated with PHITS modelling at three distinct energies, is reflected in a marked decrease in TF values.
- It is possible to analyse Σ_R by applying the knowledge of (Σ_R/ρ). As shown in **Figure 11**, density is a crucial element of quick neutron protection, and it is shown that the sample with the highest value is BG4B The results show that BG4B has exceptional neutron attenuation capabilities, with a value of 0.11 cm^{-1}.

The study concludes that the effectiveness of bioactive glasses greatly enhances the field of radiation-shielding materials. Observing the gamma and neutron radiation attenuation characteristics of three sets of bioactive glass samples with varying quantities of B_2O_3, SrO, and CaF_2 additives is the study's hypothesis. It has been demonstrated that while increasing the quantity of B_2O_3 additive improves the samples' ability to attenuate neutron radiation, increasing the amount of CaF_2 additive improves the samples' ability to attenuate gamma radiation that situation has been demonstrated using modelling with PHITS code. The data gained demonstrate that the hypothesis put forth is accurate. Additionally, this research emphasizes the vital role of targeted elemental doping in optimizing material properties to satisfy the specific requirements of various applications. Additionally, because of their improved radiation-shielding properties, these bioactive glasses provide a great deal of promise for real-world uses in situations where radiation protection is crucial.

Author Statements:

- **Ethical approval:** The conducted research is not related to either human or animal use.
- **Conflict of interest:** The authors declare that they have no known competing financial interests or personal relationships that could have appeared to influence the work reported in this paper
- **Acknowledgement:** The authors declare that they have nobody or no-company to acknowledge.
- **Author contributions:** The authors declare that they have equal right on this paper.
- **Funding information:** The authors declare that there is no funding to be acknowledged.
- **Data availability statement:** The data that support the findings of this study are available on request from the corresponding author. The data are not publicly available due to privacy or ethical restrictions.

References

[1] Hench, L. L., Splinter, R. J., Allen, W. C., & Greenlee, T. K. (1971). Bonding mechanisms at the interface of ceramic prosthetic materials. Journal of Biomedical Materials Research, 5(6), 117-141. https://doi.org/10.1002/jbm.820050611

[2] Jones, J. R., Ehrenfried, L. M., & Hench, L. L. (2006). Optimising bioactive glass scaffolds for bone tissue engineering. Biomaterials, 27(7), 964-973. https://doi.org/10.1016/j.biomaterials.2005.07.017

[3] Hench, L. L., Splinter, R. J., Allen, W. C., & Greenlee, T. K. (1971). Bonding mechanisms at the interface of ceramic prosthetic materials. Journal of Biomedical Materials Research, 5(6), 117-141. https://doi.org/10.1002/jbm.820050611

[4] Hench, L. L., & Andersson, Ö. (1993). Bioactive glasses. In An introduction to bioceramics (pp. 41-62). https://doi.org/10.1142/9789814317351_0003

[5] Carvalho, S. M., Moreira, C. D. F., Oliveira, A. C. X., Oliveira, A. A. R., Lemos, E. M. F., & Pereira, M. M. (2019). Bioactive glass nanoparticles for periodontal regeneration and applications in dentistry. In Nanobiomaterials in Clinical Dentistry (pp. 351-383). Elsevier. https://doi.org/10.1016/B978-0-12-815886-9.00015-2

[6] Hutmacher, D. W. (2000). Scaffolds in tissue engineering bone and cartilage. In The Biomaterials: Silver Jubilee Compendium, Elsevier Science, 175-189. https://doi.org/10.1016/B978-008045154-1.50021-6

[7] Rahaman, M. N., Day, D. E., Bal, B. S., Fu, Q., Jung, S. B., Bonewald, L. F., & Tomsia, A. P. (2011). Bioactive glass in tissue engineering. Acta Biomaterialia, 7(6), 2355-2373. https://doi.org/10.1016/j.actbio.2011.03.016

[8] Zhai, W., Lu, H., Chen, L., Lin, X., Huang, Y., Dai, K., Kawazoe, N., Chen, G., & Jiang, C. (2012). Silicate bioceramics induce angiogenesis during bone regeneration. Acta Biomaterialia, 8(1), 341-349.https://doi.org/10.1016/j.actbio.2011.09.008

[9] Bergmann, C., Lindner, M., Zhang, W., Koczur, K., Kirsten, A., Telle, R., et al. (2010). 3D printing of bone substitute implants using calcium phosphate and bioactive glasses. Journal of the European Ceramic Society, 30, 2563-2567.https://doi.org/10.1016/j.jeurceramsoc.2010.04.037

[10] Sergi, R., Bellucci, D., & Cannillo, V. (2020). A review of bioactive glass/natural polymer composites: state of the art. Materials, 13, 5560.https://doi.org/10.3390/ma13235560

[11] Hench, L. L., Xynos, I. D., & Polak, J. M. (2004). Bioactive glasses for in situ tissue regeneration. Journal of Biomaterials Science, Polymer Edition, 15, 543-562. https://doi.org/10.3390/ma13235560

[12] Elgayar, I., Aliev, A. E., Boccaccini, A. R., & Hill, R. G. (2005). Structural analysis of bioactive glasses. Journal of Non-Crystalline Solids, 351, 173-183. https://doi.org/10.1016/j.jnoncrysol.2004.07.067

[13] Baino, F., Fiorilli, S., & Vitale-Brovarone, C. (2016). Bioactive glass-based materials with hierarchical porosity for medical applications: review of recent advances. Acta Biomaterialia. https://doi.org/10.1016/j.actbio.2016.06.033

[14] Qiu, Q. Q., Ducheyne, P., & Ayyaswamy, P. S. (2000). New bioactive, degradable composite microspheres as tissue engineering substrates. Journal of Biomedical Materials Research. https://doi.org/10.1002/1097-4636(200010)52:1<66::AID-JBM9>3.0.CO;2-2

[15] Islam, M. T., Felfel, R. M., Abou Neel, E. A., Grant, D. M., Ahmed, I., & Hossain, K. M. Z. (2017). Bioactive calcium phosphate–based glasses and ceramics and their biomedical applications: a review. Journal of Tissue Engineering, 8. https://doi.org/10.1177/2041731417719170

[16] Bertolla, L., Dlouhý, I., Tatarko, P., Viani, A., Mahajan, A., Chlup, Z., et al. (2017). Pressureless spark plasma–sintered Bioglass®45S5 with enhanced mechanical properties and stress–induced new phase formation. Journal of the European Ceramic Society. https://doi.org/10.1016/j.jeurceramsoc.2017.02.003

[17] Al-Buriahi, M. S., & Singh, V. P. (2020). Comparison of shielding properties of various marble concretes using GEANT4 simulation and experimental data. Journal of the Australasian Ceramic Society, 1-7. https://doi.org/10.1007/s41779-020-00457-1

[18] Obaid, S., et al. (2018). Determination of gamma ray shielding parameters of rocks and concrete. Radiation Physics and Chemistry, 144, 356-360. https://doi.org/10.1016/j.radphyschem.2017.09.022

[19] Agar, O., Sayyed, M. I., Akman, F., Tekin, H. O., & Kaçal, M. R. (2019). An extensive investigation on gamma ray shielding features of Pd/Ag based alloys. Nuclear Engineering and Technology, 51, 853-859.https://doi.org/10.1016/j.net.2018.12.014

[20] Tekin, H. O., Kavaz, E., Papachristodoulou, A., Kamislioglu, M., Agar, O., Altunsoy Guclu, E. E., Kilicoglu, O., & Sayyed, M. I. (2019). Characterization of SiO2–PbO–CdO–Ga2O3 glasses for comprehensive nuclear shielding performance: alpha, proton, gamma, neutron radiation. Ceramics International, 45, 19206-19222.https://doi.org/10.1016/j.ceramint.2019.06.168

[21] Susoy, G., Altunsoy Guclu, E. E., Kilicoglu, O., Kamislioglu, M., Al Buriahi, M. S., Abuzaid, M. M., Tekin, H. O. (2020). The impact of Cr2O3 additive on nuclear radiation shielding properties of LiF–SrO–B2O3 glass system. Materials Chemistry and Physics, 242, 122481. https://doi.org/10.1016/j.matchemphys.2019.122481

[22] Tekin, H. O., Kavaz, E., Altunsoy, E. E., Kilicoglu, O., Agar, O., Erguzel, T. T., Sayyed, M. I. (2019). An extensive investigation on gamma ray and neutron attenuation parameters of cobalt oxide and nickel oxide substituted bioactive glasses. Ceramics International, 45(8),9934-9949. https://doi.org/10.1016/j.ceramint.2019.02.036

[23] Kilicoglu, O. (2019). Characterization of copper oxide and cobalt oxide substituted bioactive glasses for gamma and neutron shielding applications. Ceramics International, 45(17), 23619-23631. https://doi.org/10.1016/j.ceramint.2019.08.073

[24] Kilicoglu, O., Tekin, H. O. (2019). Bioactive glasses and direct effect of increased K2O additive for nuclear shielding performance: a comparative investigation. Ceramics International, 46(2), 1323-1333.https://doi.org/10.1016/j.ceramint.2019.09.095

[25] Al-Hadeethi, Y., Al-Buriahi, M. S., Sayyed, M. I. (2020). Bioactive glasses and the impact of Si3N4 doping on the photon attenuation up to radiotherapy energies. Ceramics International, 46(4), 5306-5314. https://doi.org/10.1016/j.ceramint.2019.10.281

[26] Almatari, M. (2017). Energy absorption and exposure buildup factors for some bioactive glasses' samples: penetration depth photon energy, and atomic number dependence. Journal of Optoelectronics and Biomedical Materials, 9, 95-105. https://chalcogen.ro/95_AlmatariM.pdf

[27] Sayyed, M. I., Manjunatha, H. C., Gaikwad, D. K., Obaid, S. S., Zaid, M. H. M., Matori, K. A., et al. (2018). Energy-absorption buildup factors and specific absorbed fractions of energy for bioactive glasses. Digest Journal of Nanomaterials and Biostructures, 13, 701-712.

[28] Syam Prasad, P., Pasha, M. B., Narasimha Rao, R., Venkateswara Rao, P., Madaboosi, N., & Özcan, M. (2024). A review on enhancing the life of teeth by toothpaste containing bioactive glass particles. *Current Oral Health Reports, 11*, 87–94.

[29] Loh, Z. W., Mohd Zaid, M. H., Awang Kechik, M. M., Yap, W. F., Amin, K. M., & Cheong, W. M. (2024). New formulation calcium-based 45S5 bioactive glass: In vitro assessment in PBS solution for potential dental applications. *Journal of Dental Materials*, *15*(2), 123–130. https://doi.org/10.1016/j.jdm.2024.04.005

[30] Mostafa, A. M. A., Uosif, M. A. M., Alrowaili, Z. A., Issa, S. A., Ivanov, V. Y., & Zakaly, H. M. (2024). Exploring the potential of strontium oxide-enriched borate bioactive glass as a bone graft material: Comprehensive analysis of physical characteristics and gamma shielding properties. Radiation Physics and Chemistry, 218, 111641.https://doi.org/10.1016/j.radphyschem.2024.111641

[31] Khattari, Z. Y., Mahdy, E. A., Salem, W. M., & Ibrahim, S. (2024). Enhancement of optical and radiation shielding properties in calcium–magnesium silicate bioactive glasses through Na2O and P2O5 additives. *Optical Materials*, *147*, 114503.https://doi.org/10.1016/j.optmat.2023.114503

[32] Deliormanlı, A. M., ALMisned, G., & Tekin, H. O. (2024). Synthesis and characterization of Nb5+ and Sm3+-doped 13–93 bioactive glass particles with improved photon transmission properties for advanced biomedical and dental applications. *Ceramics International*, *50*(17), 31211-31224.https://doi.org/10.1016/j.ceramint.2024.05.426

[33] Prasad, S., Datta, S., Adarsh, T., Diwan, P., Annapurna, K., Kundu, B., & Biswas, K. (2018). Effect of boron oxide addition on structural, thermal, in vitro bioactivity and antibacterial properties of bioactive glasses in the base S53P4 composition. Journal of Non-Crystalline Solids, 498, 204-215.https://doi.org/10.1016/j.jnoncrysol.2018.06.027

[34] Liang, W., Rüssel, C., Day, D. E., & Völksch, G. (2006). Bioactive comparison of a borate, phosphate and silicate glass. Journal of Materials Research, 21, 125-131. https://doi.org/10.1557/jmr.2006.0025

[35] Rahaman, M. N., Day, D. E., Bal, B. S., Fu, Q., Jung, S. B., Bonewald, L. F., & Tomsia, A. P. (2011). Bioactive glass in tissue engineering. Acta Biomaterialia, 7, 2355-2373.https://doi.org/10.1016/j.actbio.2011.03.016

[36] Balasubramanian, P., Büttner, T., Pacheco, V. M., & Boccaccini, A. R. (2018). Boron-containing bioactive glasses in bone and soft tissue engineering. Journal of the European Ceramic Society, 38, 855-869. https://doi.org/10.1016/j.jeurceramsoc.2017.11.001

[37] Newnham, R. E. (1991). Agricultural practices affect arthritis. Nutrition and Health, 7, 89-100. https://doi.org/10.1177/026010609100700204

[38] Moseman, R. F. (1994). Chemical disposition of boron in animals and humans. Environmental Health Perspectives, 102, 113. https://doi.org/10.1289/ehp.94102s7113

[39] Newnham, R. E. (1994). Essentiality of boron for healthy bones and joints. Environmental Health Perspectives, 102, 83. https://doi.org/10.1289/ehp.94102s783

[40] Chapin, R. E., Ku, W. W., Kenney, M. A., McCoy, H. (1998). The effects of dietary boric acid on bone strength in rats. Biological Trace Element Research, 66, 395-399. https://doi.org/10.1007/BF02783150

[41] Satyanarayana, T., Vasu Babu, M., Nagarjuna, G., Rama Koti Reddy, D. V., Venkateswara Rao, P., & Syam Prasad, P. (2017). Structural investigations on P2O5-CaO-Na2O-K2O: SrO bioactive glass ceramics. Ceramics International, 43(13), 10144-10150. https://doi.org/10.1016/j.ceramint.2017.05.037

[42] Xue, W., Moore, J. L., Hosick, H. L., Bose, S., Bandyopadhyay, A., Lu, W. W., Cheung, K. M., Luk, K. D. (2006). Osteoprecursor cell response to strontium-containing hydroxyapatite ceramics. Journal of Biomedical Materials Research, 79, 804.https://doi.org/10.1002/jbm.a.30815

[43] Tian, M., Chen, F., Song, W., Song, Y., Chen, Y., Wan, C., Yu, X., & Zhang, X. J. (2009). In vivo study of porous strontium-doped calcium polyphosphate sintered discs for bone substitute applications. Journal of Materials Science: Materials in Medicine, 20, 1505-1512. https://doi.org/10.1007/s10856-009-3713-5

[44] Bellucci, D., Sola, A., Cacciotti, I., Bartoli, C., Gazzarri, M., Bianco, A., Chiellini, F., & Cannillo, V. (2014). Mg and/or Sr-doped tricalcium phosphate/bioactive glass composites: Synthesis, microstructure and biological responsiveness. Materials Science & Engineering C, 42, 312-324. https://doi.org/10.1016/j.msec.2014.05.047

[45] Zhang, W., Shen, Y., Pan, H., Lin, K., Liu, X., Darvell, B., Lu, W., Chang, J., Deng, L., Wang, D., & Huang, W. (2011). Effects of strontium in modified biomaterials. Acta Biomaterialia, 7(2), 800-808. https://doi.org/10.1016/j.actbio.2010.08.031

[46] Dziadek, M., Zagrajczuk, B., Menaszek, E., Wegrzynowicz, A., Pawlik, J., & Cholewa-Kowalska, K. (2016). Gel–derived SiO2–CaO–P2O5 bioactive glasses and glass ceramics modified by SrO addition. Ceramics International, 42, 5842-5857.https://doi.org/10.1016/j.ceramint.2015.12.128

[47] Gentleman, E., Fredholm, Y. C., Jell, G., O'Donnell, M. D., Hill, R. G., & Stevens, M. M. (2010). The effects of strontium-substituted bioactive glasses on osteoblasts and osteoclasts in vitro. Biomaterials, 31, 3949-3956. https://doi.org/10.1016/j.biomaterials.2010.01.121

[48] Goel, A., Rajagopal, R. R., & Ferreira, J. M. F. (2011). Influence of strontium on structure, sintering and biodegradation behaviour of CaO–MgO–SrO–SiO2–P2O5–CaF2 glasses. Acta Biomaterialia, 7, 4071-4080. https://doi.org/10.1016/j.actbio.2011.06.047

[49] Isaac, J., Nohra, J., Lao, J., Jallot, E., Nedelec, J. M., Berdal, A., & Sautier, J. M. (2011). Effects of strontium-doped bioactive glass on the differentiation of cultured osteogenic cells. European Cells & Materials, 21, 130-143. https://doi.org/10.22203/ecm.v021a11

[50] Rajkumar, G., Dhivya, V., Mahalaxmi, S., Rajkumar, K., Sathishkumar, G. K., & Karpagam, R. (2018). Influence of fluoride for enhancing bioactivity onto phosphate-based glasses. Journal of Non-Crystalline Solids, 493, 108-118. https://doi.org/10.1016/j.jnoncrysol.2018.04.046

[51] Brauer, D. S., Karpukhina, N., Law, R. V., & Hill, R. G. (2009). Structure of fluoride-containing bioactive glasses. Journal of Materials Chemistry, 19(31), 5629-5636. https://doi.org/10.1039/B900956F

[52] Biswas, R., Sahadath, H., Mollah, A. S., & Huq, M. F. (2016). Calculation of gamma-ray attenuation parameters for locally developed shielding material: Polyboron. Journal of Radiation Research and

Applied Sciences, 9(1), 26–34. https://doi.org/10.1016/j.jrras.2015.08.005

[53] Şakar, E., Özpolat, Ö. F., Alım, M. I. B., & Sayyed, M. K. (2020). Phy-X / PSD: Development of a user-friendly online software for calculation of parameters relevant to radiation shielding and dosimetry. Radiation Physics and Chemistry, 166, Article 108496.https://doi.org/10.1016/j.radphyschem.2019.108496

[54] Sato, T., Iwamoto, Y., Hashimoto, S., Ogawa, T., Furuta, T., Abe, S.-i., Kai, T., Tsai, P.-E., Matsuda, N., Iwase, H., et al. (n.d.). Features of particle and heavy ion transport code system (PHITS) version 3.02. https://doi.org/10.1080/00223131.2017.1419890

[55] Niita, K., et al. (2006). PHITS—a particle and heavy ion transport code system. Radiation Measurements, 41(9–10), 1080–1090.https://doi.org/10.1016/j.radmeas.2006.07.013

[56] Agar, O., Sayyed, M. I., Akman, F., Tekin, H. O., & Kaçal, M. R. (2019). An extensive investigation on gamma ray shielding features of Pd/Ag-based alloys. Nuclear Engineering and Technology, 51, 853–859. https://doi.org/10.1016/j.net.2018.12.014

[57] Jackson, D. F., & Hawkes, D. J. (1981). X-ray attenuation coefficients of elements and mixtures. Physics Reports, 70, 169–233. https://doi.org/10.1016/0370-1573(81)90014-4

[58] Tekin, H. O., Kilicoglu, O., Kavaz, E., Altunsoy, E. E., Almatari, M., Agar, O., & Sayyed, M. I. (2017). The investigation of gamma-ray and neutron shielding parameters of Na2O-CaO-P2O5-SiO2 bioactive glasses using MCNPX code. Results in Physics, 12, 1797–1804. https://doi.org/10.1016/j.rinp.2019.02.017

[59] Akman, F., Geçibesler, I. H., Demirkol, I., & Çetin, A. (2018). Determination of effective atomic numbers and electron densities for some synthesized triazoles from the measured total mass attenuation coefficients at different energies. Canadian Journal of Physics, 97(1), 86–92. https://doi.org/10.1139/cjp-2017-0923

[60] Hine, G. J. (1952). The effective atomic numbers of materials for various gamma ray interactions. Physical Review, 85, 725.

[61] Yılmaz Alan, H. (2024). A Study on the Effect of Addition Li, Na, and K on the Radiation Shielding Capabilities of B2O3-TeO2-ZnO-PbF2-Er2O3 Glass Structure. Afyon Kocatepe Üniversitesi Fen Ve Mühendislik Bilimleri Dergisi, 24(4), 789-797. https://doi.org/10.35414/akufemubid.1411091

[62] Almisned, Baykal Sen, D., Alkarrani, H., Susoy, G., Tekin, H.O., (2024). Advancing mechanical durability and radiation shielding properties in Silicon dioxide (SiO2) glasses through various incorporations: A comparative analysis. *Journal of Non-Crystalline Solids Advances*, *17*, 100232.https://doi.org/10.1016/j.jnoncrysoladv.2024.100232

[63] Süsoy Doğan, G. (2020). Lithium-boro-tellurite glasses with ZnO additive: Exposure Buildup Factors (EBF) and Nuclear Shielding Properties. *Avrupa Bilim Ve Teknoloji Dergisi*(*18*), 531-544. https://doi.org/10.31590/ejosat.697254